Journal of Nuclear Materials 395 (2009) 112–119

Contents lists available at ScienceDirect

Journal of Nuclear Materials

journal homepage: www.elsevier.com/locate/jnucmat

Derivation of potential model for $LiAlO_2$ by simple and effective optimization of model parameters

H. Tsuchihira *, T. Oda, S. Tanaka

Department of Nuclear Engineering and Management, The University of Tokyo, Hongo 7-3-1, Bunkyo-ku, Tokyo 113-0033, Japan

ARTICLE INFO

Article history:
Received 10 March 2009
Accepted 2 October 2009

PACS:
28.52.Fa
34.20.Cf
61.43.Bn

ABSTRACT

Interatomic potentials of $LiAlO_2$ were constructed by a simple and effective method. In this method, the model function consists of multiple inverse polynomial functions with an exponential truncation function, and parameters in the potential model can be optimized as a solution of simultaneous linear equations. Potential energies obtained by *ab initio* calculation are used as fitting targets for model parameter optimization. Lattice constants, elastic properties, defect-formation energy, thermal expansions and the melting point were calculated under the constructed potential models. The results showed good agreement with experimental values and *ab initio* calculation results, which underscores the validity of the presented method.

1. Introduction

Solid breeding materials are required to supply tritium adequately and rapidly, and to be compatible with structural materials. From these viewpoints, ternary lithium-containing oxides such as Li_2TiO_3, Li_4SiO_4 and $LiAlO_2$ are regarded as candidates. However, the generation and annihilation behaviors of irradiation defects in these materials, which should affect tritium release behavior [1,2] and material properties [3], are not understood sufficiently.

Classical molecular dynamics (MD) method is a powerful technique used to simulate displacement cascades in atomic scale, which are difficult to observe by experiment. Construction of reliable potential models representing interaction between atoms is a key step to acquire reasonable simulation results. In this study, we therefore aimed to establish a construction method of a potential model for ternary lithium oxides, which can be applied to irradiation simulation in the future.

In general, a potential model can be created by defining a model function based on physics consideration and then by adjusting model parameters to reproduce experimental values such as lattice constants. However, a potential model derived by this method guarantees only motion of atoms near the ideal structure basically. Hence, this method is not suitable to create a potential model employed in irradiation simulation.

Alternatively, results of *ab initio* calculation have also been used for a fitting target to which the potential model is fitted, coupled with great development of the accuracy of *ab initio* calculation. It is an advantage of this method that many fitting targets including potential energies in heavily distorted structures, which could emerge at high temperatures or in systems suffered irradiation damage, are obtainable under constant conditions [4].

However, a larger number of fitting targets make fitting procedures more difficult, mainly for two reasons. One reason is that it is usually necessary to solve a nonlinear equation to optimize model parameters. An obtained solution in a nonlinear equation is not guaranteed to be the global minimum. Therefore, multiple trials and errors are required. Even parameters having achieved a criterion include an arbitrary nature; thus systematic discussion about fitting error is difficult. The other reason is that it is fundamentally difficult to obtain reasonable fitting to numerous targets using simple model functions such as the Buckingham model, which has been widely applied for ionic crystals. These two points must be improved to create good potential models based on results of *ab initio* calculation.

The construction method of a potential model in the present paper has two features to solve the problems described above. One is that model parameters can be determined uniquely as a solution of simultaneous linear equations. The other is that the model function enables extension of its own partial function space systematically. In order to achieve these requirements, we utilized a model function comprising multiple inverse polynomial functions with an exponential truncation function.

Potential models of $LiAlO_2$ were constructed to validate our method. Because this material has relatively simple crystal

* Corresponding author. Address: Eng. Build. 8 #430, Hongo 7-3-1, Bunkyo-ku, Tokyo 113-0033, Japan. Tel: +81 3 5841 6970; fax: +81 3 5841 8713.
E-mail address: tsuchihira@flanker.q.t.u-tokyo.ac.jp (H. Tsuchihira).

0022-3115/$ - see front matter © 2009 Elsevier B.V. All rights reserved.
doi:10.1016/j.jnucmat.2009.10.041

structure and strong ionicity among ternary lithium-containing oxides, even a pairwise potential model is expected to describe this material acceptably. Hence, we regard this material is appropriate for use as a test material.

The present paper is organized into four sections; in Section 2, the construction method of potential models and the evaluation method of constructed potential models are presented. Potential energies evaluated using *ab initio* calculations were used as fitting targets for model parameter optimization. We verify the effectiveness of our methodology in Section 3 through comparison of material properties evaluated by MD and molecular statics (MS) simulation under constructed potential models with these experimental values or *ab initio* calculation values. Furthermore, limitations and shortcomings of the present model are discussed at the end of Section 3. Finally, the paper is closed by Section 4 with concluding remarks.

2. Method

2.1. Ab initio calculation

For fitting targets of our potential models, potential energies in various distorted crystal structures were evaluated using the CASTEP code [5] of plane-wave pseudopotential DFT calculation with the GGA-PBE functional [6]. Pseudopotentials implemented in the CASTEP code were used. The energy cut-off and Monkhorst–Pack grid for k-point sampling were set, respectively, to 380 eV and $5 \times 5 \times 4$. The primitive cell (4 $LiAlO_2$) under periodic boundary conditions (PBC) was used as the unit cell. In the present paper, the term "PBC" shall mean three-dimensional PBC. All calculations were done in spin-restricted conditions.

Four types of distortion were adopted: (i) displacement of one Li, Al or O ion along the x, y, or z axis (x and z axis for Li, x, and z axis for Al, and x, y, and z axis for O, because of omissions of equivalent displacements in light of the lattice symmetry); (ii) expansion and contraction of the lattice constant (isotropic and anisotropic changes of seven kinds); (iii) displacement of one ion toward another ion (with short interatomic distance combinations of 19 kinds); and (iv) mixture of (i) and (ii) (641 kinds). Each kind of distortion had several different degrees of distortion. Consequently, the number of structures used in calculations came to 2158 in all.

DFT calculation is also utilized to evaluate elastic properties and the formation energy of a Li Frenkel pair in $LiAlO_2$. The energy cut-off and the k-point sampling grid were set as described above. In determination of elastic properties, first, all coordinates of atoms are re-optimized in a cell that is deformed according to a specific strain tensor. Then, the corresponding stress tensor is obtained, and elastic properties are determined from strain–stress relations, as successfully applied to Li_2O [7] or $MgSiO_3$ [8]. The formation energy of a Li Frenkel pair was evaluated by using $2 \times 2 \times 2$ supercell (32 $LiAlO_2$) under PBC. These results were used in validation of constructed potential models.

2.2. Potential model

We adopted a pairwise potential model for simplicity, with reliance on high ionicity of $LiAlO_2$. Our pairwise potential model between two ions is expressed as

$$U_k(r) = \frac{q_1 q_2}{r} + \exp(-r) \times \sum_{n=N_0}^{N_0+N-1} \left(a_{kn} \times \frac{1}{r^n} \right) \quad (1)$$

where q_1 and q_2 are effective charges, r (Å) an interatomic distance, and N_0, N and a_{kn} (eV Å^n) the smallest power, the number of inverse polynomial functions, and the coefficient of each term, respectively. The subscript k of U_k and a_{kn} indexes atom–atom combination: k = 1, 2, 3, 4, 5 and 6 for Li–Li, Li–O, Li–Al, O–O, O–Al and Al–Al, respectively. The Coulombic term was evaluated using Ewald summation technique [9], while the remaining terms were calculated directly with the cut-off distance of 10 Å. The remaining terms are inverse polynomials of an interatomic distance, which have different coefficients and which are multiplied by $\exp(-r)$ to improve convergence to 0 over long distances.

The validity of potential models is fundamentally not guaranteed in regions where an interionic distance is shorter than that in the structures of which potential energies were included in the fitting targets. Therefore, the ZBL potential model [10], which is suggested in atom/ion collision theory, was adopted for these regions. The ZBL potential model is expressed as

$$U_{\mathrm{ZBL}}(r) = \frac{Z_i Z_j}{r} \varphi\left(\frac{r}{a}\right)$$

with $\varphi(x) = 0.1818e^{-3.2x} + 0.5099e^{-0.9423x} + 0.2802e^{-0.4028x} + 0.02817e^{-0.2016x}$, and

$$a = \frac{0.8854 a_{\mathrm{bohr}}}{Z_i^{0.23} + Z_j^{0.23}} \quad (2)$$

Here, Z_i, Z_j and a_{bohr} are atomic number of atom i and j and Bohr radius, respectively. The ZBL potential models and Eq. (1) were connected by fifth-order inverse polynomials to conserve consistency at the connection points up to the second derivative. The inverse polynomial is written as

$$U_{k\_\mathrm{fifth}}(r) = \sum_{l=0}^{5} \left(b_{kl} \times \frac{1}{r^l} \right) \quad (3)$$

where b_{kl} is the coefficient of each term. The subscript k is the same as in Eq. (1). Table 1 shows the connection radius between the ZBL potential and fifth-order inverse polynomials (r_α), and the connection radius between fifth-order inverse polynomials and Eq. (1) (r_β), as well as the minimum interatomic distance among all the interatomic distances in all the structures included in the fitting targets (r_n), and the minimum interatomic distance in the structure optimized by *ab initio* calculation (r_e) for each combination.

In Table 1, r_β (2.30 Å) is longer than r_n (2.09 Å) for O–O combination. When r_β was set to be shorter than 2.30 Å, the fifth-order inverse polynomial took an extreme value between r_α and r_β, although it is expected to decrease monotonically in this distance range. Therefore, r_β was set to 2.30 Å with which no extreme value was observed in the fifth-order inverse polynomial. Since the difference of the potential energy at 2.09 Å between the original potential model and the fifth-order inverse polynomial was 0.24 eV, we regard that it is not so problematic.

Table 1
Connection radius between ZBL potential and fifth-order inverse polynomials (r_α), and the connection radius between fifth-order inverse polynomials and Eq. (1) (r_β), along with the minimum interatomic distance among all the interatomic distances contained in the structures included in the fitting targets (r_n) and the minimum distance in the structure optimized by *ab initio* calculation (r_e) for each combination.

	r_α (Å)	r_β (Å)	r_n (Å)	r_e (Å)
Li–Li	0.50	1.40	2.10	3.06
Li–O	0.50	1.20	1.44	1.94
Li–Al	0.50	1.30	1.87	2.63
O–O	0.50	2.30	2.09	2.81
O–Al	0.50	1.20	1.19	1.73
Al–Al	0.50	1.60	1.91	3.08

2.3. Fitting method

Fitting to the results of *ab initio* calculation is expressed as a minimization problem of the square sum of fitting errors (F) written as

$$F = \sum_{m=1}^{M} \left(E_m^{\mathrm{DFT}} - E_m^{\mathrm{PM}} \right)^2 = \sum_{m=1}^{M} \left(E_m^{\mathrm{DFT}} - \sum_{k=1}^{6} \sum^{r_{m\_k} < r_{\mathrm{cut}}} U_k(r_{m\_k}) \right)^2 \tag{4}$$

where E_m^{DFT} and E_m^{PM}, respectively signify the potential energy evaluated by *ab initio* calculation and the potential energy predicted using the potential model in the same mth structure, r_{m_k} an interatomic distance of atom–atom combination k (k = 1, 2, 3, 4, 5 and 6 for Li–Li, Li–O, Li–Al, O–O, O–Al and Al–Al, respectively) in the mth structure, r_{cut} the cut-off distance, and M the number of structures used in calculations: 2158 in this study.

Treated as fitting parameters, q in Eq. (1) became larger than the formal charge of each ion. Consequently, the results of Mulliken population analysis [11] in the optimized $LiAlO_2$ structure were adopted as fixed values of ionic charges: +0.7e for Li^+, −1.1e for O^{2-} and +1.5e for Al^{3+}, respectively. As the plane-wave basis set is not a localized basis set, the CASTEP code projects the optimized plane-wave states onto a Linear Combination of Atomic Orbitals (LCAO) basis set in the population analysis. One may think that this method has two problems. First, the results of population analysis do not have sufficient physical background. Although there are some calculation methods other than Mulliken population analysis to estimate ionic charges such as Bader analysis [12], it is basically difficult to obtain ionic charges with an adequate background by any methodology. In the present work, we utilized the population analysis for simplicity. It should be noted that as far as partial charges were applied (e.g. +0.6e for Li^+, −1.2e for O^{2-} and +1.8e for Al^{3+}), the quality of created potential models was similar to that described in the present paper, and was better than that of the full charge model (+1e for Li^+, −2e for O^{2-} and +3e for Al^{3+}). Second, population analysis result depends on structure. Nonetheless, we consider that it is appropriate to use the values evaluated in the optimized structure as representative values of the first approximation. This consideration would be supported by the fact that the values in the optimized structures lie near the middle between the maximum and the minimum values in all the structures of which potential energies were used as the fitting targets (Table 2).

Furthermore, N_0 and N were also predetermined to make the minimization problem of F in Eq. (4) to be simultaneous linear equations. Finally, an extreme value of F is given with a set of a_{kn} that satisfies the following equation.

$$\frac{\partial F}{\partial a_{kn}} = \sum_{i=1}^{6} \sum_{j=N_0}^{N_0+N-1} \left[a_{ij} \times \sum_{m=1}^{M} \left\{ \left(\sum^{r_{m\_k} < r_{\mathrm{cut}}} \frac{1}{r_{m\_k}^n} \right) \left(\sum^{r_{m\_j} < r_{\mathrm{cut}}} \frac{1}{r_{m\_i}^j} \right) \right\} \right] + \sum_{m=1}^{M} \left\{ \left(\sum^{r_{m\_k} < r_{\mathrm{cut}}} \frac{1}{r_{m\_k}^n} \right) E_m^{\mathrm{DFT}} \right\} = 0 \tag{5}$$

Setting up Eq. (5) for all six (the number of atom–atom combinations – Li–Li, Li–O, Li–Al, O–O, O–Al and Al–Al) × N combinations gives 6N order simultaneous equations with respect to a set of a_{kn}. A set of a_{kn} is linearly independent and F diverges obviously to $+\infty$ when an a_{kn} diverges to $\pm\infty$. Moreover, it was confirmed that the simultaneous equations were linearly independent. Therefore, the obtained extreme value is expected to be the minimum value. This model enables extension of the partial function space of the model function systematically, by changing the number of inverse polynomial functions. However, it should be noted that a parameter set determined by this procedure depends on N_0 and N, which were predetermined so as to make the minimization problem to be simultaneous linear equations. The influence of the pre-determined parameters will be discussed in Section 3.

Table 2
Effective charge of each atom obtained by population analysis of *ab initio* calculation.

	Li	O	Al
Optimized (e)	0.70	−1.10	1.50
Maximum (e)	0.97	−0.62	1.88
Minimum (e)	0.37	−1.34	0.41

2.4. Evaluation method of material properties

Using the obtained potential models, (i) lattice constants and elastic properties (the elastic constants, the bulk modulus, Young's modulus and Poisson's ratio by MS), (ii) formation energy of a Li Frenkel pair (by MS), (iii) thermal expansion (by MD) and (iv) melting point (by MD) were calculated. Then, in comparison to DFT calculation values obtained in the present research or reported experimental values, the validity of potential models was checked.

The GULP code [13] was used for MS calculation. The primitive cell (4 $LiAlO_2$) under PBC was used as the system. The formation energy of a Li Frenkel pair was evaluated by using 2 × 2 × 2 supercell (32 $LiAlO_2$) under PBC.

The DL_POLY code [14] was used in the MD calculation. For determination of the thermal expansion coefficients, a 5 × 5 × 5 supercell (500 $LiAlO_2$) was used under PBC. Each calculation was conducted under Berendsen NPT [15] ensemble (anisotropic barostat). The time step was set to 1 fs. After an equilibration run for 50 ps, a production run was performed for 150 ps at each temperature.

The melting point was estimated by direct simulation of the liquid/solid interface [16]. The interface was constructed by combining two separate simulation cells of a solid structure and a liquid structure, respectively, near an estimated melting point. Therefore, the combined cell is a 5 × 5 × 10 supercell (1000 $LiAlO_2$) having the interface of (0 0 1) plane at the middle along [0 0 1] direction. PBC was imposed on the system. The cell vectors were fixed at the equilibrium values achieved in a solid simulation conducted for determination of the thermal expansion coefficient described above. Then, MD simulations were performed at 1900, 2000, and 2100 K under Berendsen NVT ensemble in order to check movement of the interface. The temperature at which solid and liquid structures coexist in balance is regarded as the melting point.

3. Results and discussion

3.1. Evaluation of optimized parameters

Initially, the effects of pre-determined parameter N on minimization of F were investigated. First, N_0 in Eq. (1) was set to 4. The increase of F and improvement of elastic properties were observed when N_0 = 3 was applied. On the other hand, when N_0 = 5 was applied, decreased F and deterioration of elastic properties were observed. Therefore, we applied N_0 = 4 because of the balance between F and elastic properties in this study.

Fig. 1 shows the N dependency of F. The blue circle represents the finally adopted parameter for this research. It is reasonable that larger N caused smaller F because the partial function space spanned by potential functions is expanded by the increase of N. However, multiple extreme values were observed when N was larger than 7. Fig. 2 shows O–O potentials in N = 5, 6, and 7. No extreme value was observed in N = 5 and 6, although two were observed in N = 7. The interaction of O–O is strongly repulsive by the Coulomb force. Therefore, monotonic decrease is expected in this distance range.

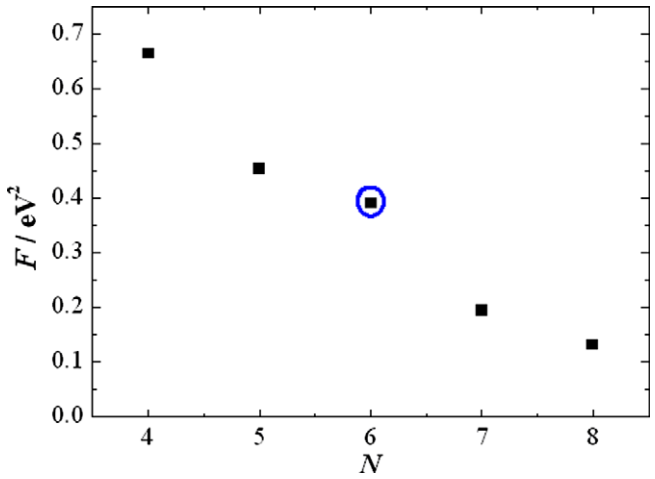

Fig. 1. N dependence of F.

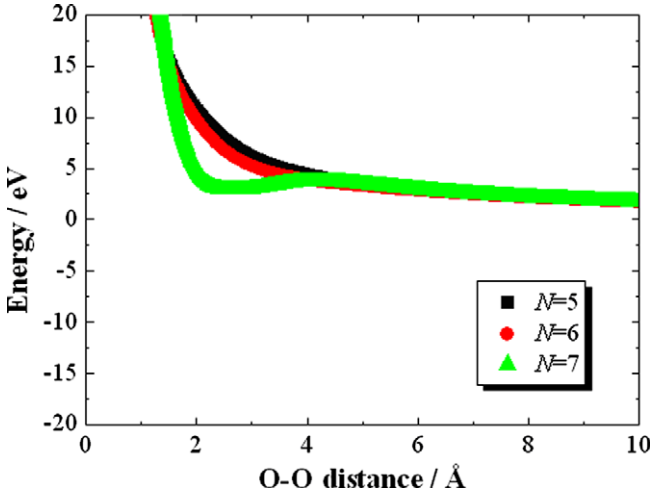

Fig. 2. O–O interatomic potentials with $N = 5$, 6, or 7.

The observed extreme values were attributed to the fact that a part of interaction that is expected to be described by many-body interactions is expressed forcibly by pairwise potential, similarly to the potential model obtained by Izvekov et al. [17]. By counting extreme values and the effect to reduce F, $N = 6$ was adopted in this research. Note that improper extreme values at $N = 7$ were observed only in the O–O potential. It is considered that interactions involved with O ions are affected strongly by many-body interactions because the directional 2p orbital mainly contributes.

From the previous discussion, we adopted the model parameters of $N = 6$ and $N_0 = 4$. Under these conditions, a set of a_{kn} in Eq. (5) and b_{kl} in Eq. (3) was obtained as given in Tables 3 and 4, respectively. The interatomic potential curves are shown in Fig. 3(a) and (b). Perpendicular lines represent the minimum interatomic distances in the structure optimized by *ab initio* calculation (r_e).

Fig. 4(a)–(c) show typical examples of fitting quality in distortions of three kinds: (a) displacement of the Li1 atom along the x direction, (b) isotropic lattice expansion and contraction, and (c) displacement of O1 atom towards the Li2 atom (refer to Fig. 5 about the label of each atom). In addition to these three cases, similar fitting qualities were achieved in all cases.

In the following, some material properties that were simulated using the constructed potential model are verified.

3.2. Lattice constant and elastic properties

Table 5 shows lattice constants and elastic properties of MS calculation under the constructed potential models, *ab initio* calculation and experiment. It is noted that the experimental values of bulk modulus were evaluated from the experimental values of elastic constants by using Voigt's formula [21] in the present study. Because the crystal lattice of $LiAlO_2$ is tetragonal, Voigt's formula becomes the following expression:

$$K = \frac{1}{9}(2C_{11} + 2C_{12} + 4C_{13} + C_{33}) \tag{6}$$

where K is the bulk modulus and C_{ij} the elastic constants.

In order to assess the fitting quality of potential models, agreement of potential-model values with DFT values is more important than that with experimental values, because the fitting targets were the potential energies calculated by DFT in the present study. Moreover, agreement with experimental values is usually acquired when agreement with DFT values is achieved, because DFT values basically give good agreement with experimental values, as shown in Table 5. Hereafter, therefore, we mainly discuss agreement/disagreement of potential-model values with DFT values.

Table 3
Optimized a_{kn} (the parameters of the potential model described by Eq. (4)).

k	1(Li–Li)	2(Li–O)	3(Li–Al)	4(O–O)	5(O–Al)	6(Al–Al)
a_{k4} (eV Å^4)	4521.76	3601.43	7046.13	−294593.48	−792.21	229744.63
a_{k5} (eV Å^5)	−29903.50	−23355.31	−41279.19	3207600.64	−2679.98	−1990630.59
a_{k6} (eV Å^6)	78671.25	60000.90	92587.30	−14056775.34	19246.18	7008353.84
a_{k7} (eV Å^7)	−102207.73	−75546.45	−93483.34	30870104.82	−32506.78	−12450938.27
a_{k8} (eV Å^8)	65407.83	46612.24	36821.62	−33833115.12	21760.98	11121900.42
a_{k9} (eV Å^9)	−16480.68	−11278.17	−1389.97	14745422.13	−4897.01	−3986404.96

Table 4
Optimized b_{kl} (the parameters of the potential model described by Eq. (2)).

k	1(Li–Li)	2(Li–O)	3(Li–Al)	4(O–O)	5(O–Al)	6(Al–Al)
b_{k0} (eV)	−43.31	−101.16	147.48	−11.70	578.71	−175.77
b_{k1} (eV Å)	189.25	467.36	−584.21	71.13	−2133.10	798.21
b_{k2} (eV Å^2)	−281.29	−868.50	933.82	−88.66	2772.12	−1193.18
b_{k3} (eV Å^3)	199.57	742.06	−690.32	67.09	−1647.36	857.57
b_{k4} (eV Å^4)	−63.58	−279.69	254.69	−4.36	494.50	−248.36
b_{k5} (eV Å^5)	7.78	39.51	−35.68	−1.61	−57.86	27.61

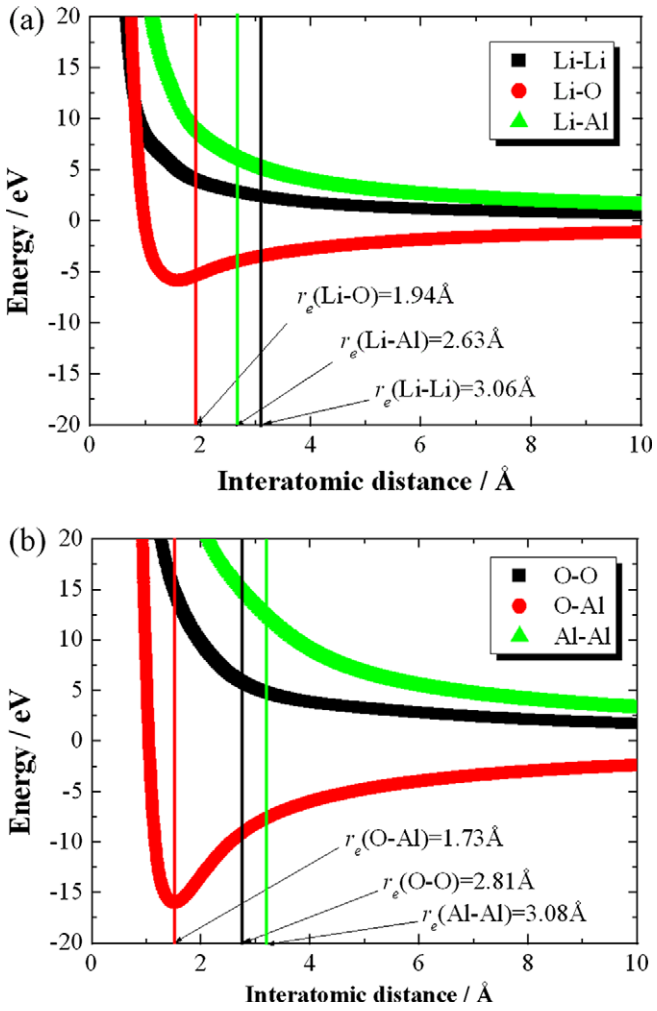

Fig. 3. Constructed interatomic potentials: r_e corresponds to the shortest distance in the structure optimized by *ab initio* calculation for each combination.

In Table 5, some properties showed significant disagreement. As examples, overestimation of Poisson's ratios *xy*, *xz*, and underestimation of *zx* were observed. This disagreement arose even under the other potential models obtained with different pre-determined parameters (see Section 3.1). Hence, it could result mainly from a lack of many-body interactions in the present potential model, as the importance of three-body forces has been confirmed for ternary lithium oxides, e.g. $LiNbO_3$ [22]. Except this, most properties such as the elastic properties and the lattice constants are comparable between potential-model values and DFT values.

3.3. Defect-formation energy

The formation energy of a Li Frenkel pair was evaluated to be 3.07 and 2.92 eV by constructed potential models and DFT calculation, respectively. The two values showed good agreement.

When the defect is formed, some interatomic distances become shorter than that of optimized structure. The appropriate result of defect-formation energy can derive from the fact that fitting targets include potential energies in structures that contain shorter interatomic distances, similar to circumference of interstitial atoms, than that of the optimized structure.

3.4. Thermal expansion

Fig. 6 shows the temperature dependence of the expansion ratio of *a* and *c* lattice constants. They were evaluated using MD from

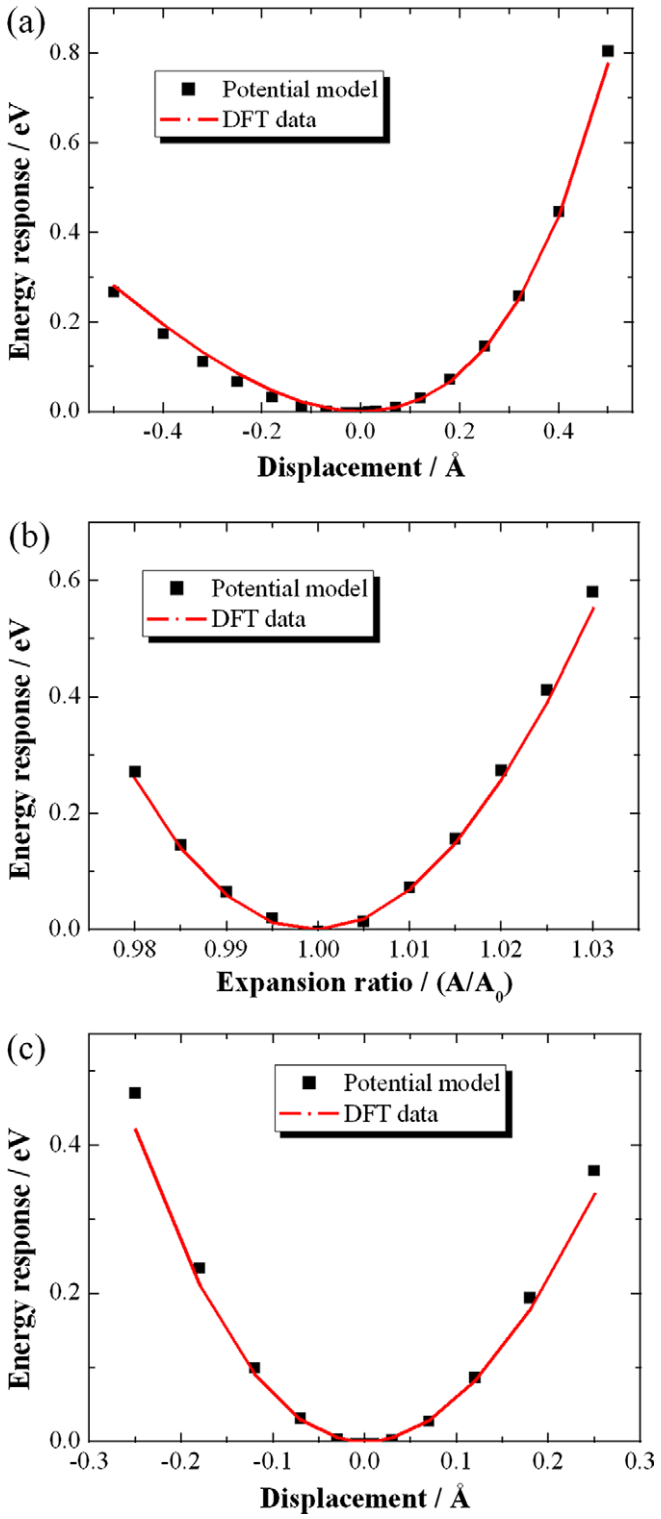

Fig. 4. Potential energy response of (a) Li1 atom displaced by −0.5–0.5 Å along the *x* direction, (b) isotropic lattice expansion and contraction by 98–103%, and (c) O1 atom displaced −0.25–0.25 Å towards the Li2 atom.

the average values of lattice constants for 150 ps production run after 50 ps equilibration run at each temperature. Table 6 shows linear expansion coefficients evaluated from Fig. 6, together with those evaluated experimentally. The calculation results are obtained from the slope of least-square fitted straight line over 0–2600 K. The calculated values are comparable to the experimental values. In most potential models that were constructed with different

Table 5
Lattice constants and elastic properties. PM and DFT indicate values evaluated under the constructed potential model and *ab initio* calculation, respectively.

		PM	DFT	Exp.
Lattice constant (Å)	a	5.12	5.12	5.17 [18]
	c	6.17	6.18	6.26 [18]
Elastic constant (GPa)	C_{11}	128.4	158.0	173.2 [19], 161.8 [20]
	C_{12}	76.2	61.7	26.1 [19], 74.1 [20]
	C_{13}	88.8	65.0	48.8 [19], 73.9 [20]
	C_{33}	203.6	177.2	176.2 [19], 194.7 [20]
	C_{44}	50.2	68.6	64.3 [20]
	C_{66}	54.3	66.0	35.5 [20]
Bulk modulus (GPa)		100.9	97.0	85.6 [19], 106.9 [20]
Young's modulus (GPa)	X, Y	74.0	123.4	–
	Z	126.6	138.7	–
Poisson's ratio	xy, yx	0.418	0.282	–
	xz, yz	0.434	0.263	–
	zx, zy	0.254	0.296	–

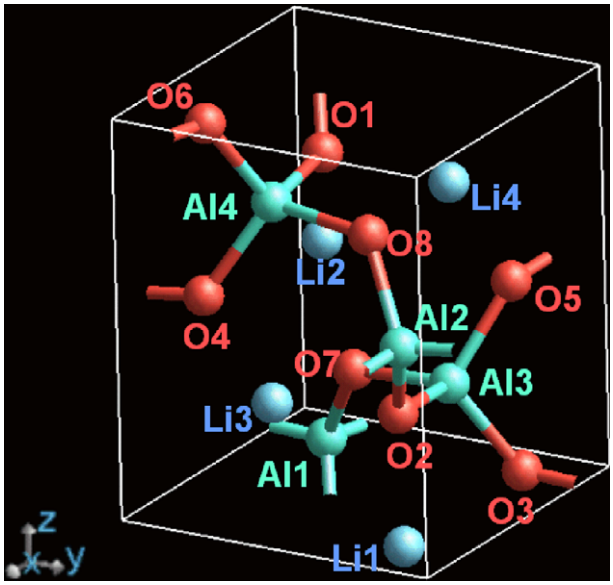

Fig. 5. Optimized $LiAlO_2$ structure.

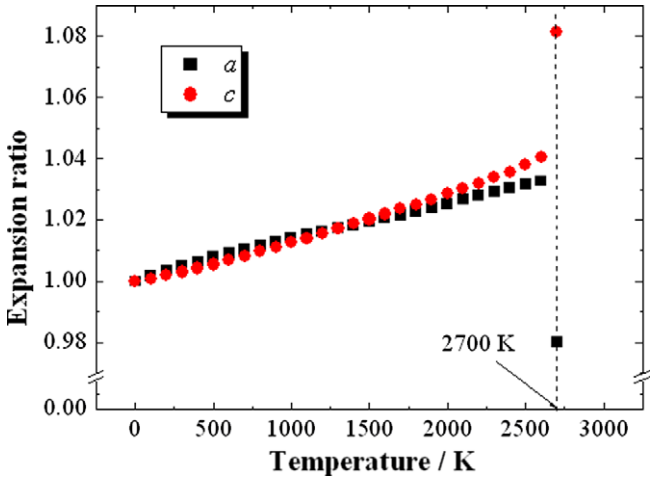

Fig. 6. Temperature dependence of the expansion ratio.

pre-determined parameters (see Section 3.1) and had a small fitting error, the thermal expansions were well predicted. The high accuracy of MD simulation at high temperatures can result from the fact that potential energies of structures in which atoms are largely displaced were added to fitting targets, because interatomic distances vary strongly at high temperatures.

Table 6
Linear expansion coefficient.

	Lattice	PM	Exp.
Linear expansion coefficient (10^{-5} K^{-1})	a	1.3	1.5 [18], 1.7 [23]
	c	1.4	0.7 [18], 1.0 [23]

From the discontinuity of thermal expansion ratio, the melting point can be guessed to be 2700 K in Fig. 6. However, this evaluation method usually overestimates the melting point because of a nucleation barrier to melting derived from liquid/solid interface energy [24]. A more appropriate method to determine the melting point suggested firstly by Ladd and Woodcock [25] is applied in Section 3.5.

3.5. Melting point

Fig. 7(a)–(c) show the atomic configurations of the system of $5 \times 5 \times 10$ supercell, which initially had the solid/liquid interfaces of (0 0 1) plane at the edge and the middle along [0 0 1] direction. These snapshots were acquired after MD simulation of 1 ns at 1900, 2000 and 2100 K. Fig. 7(a) and Fig. 7(c) have no solid–liquid interface because the systems totally became solid and liquid, respectively. On the other hand, Fig. 7(b) still has the solid–liquid interfaces represented by the yellow dashed lines. Therefore, the melting point is indicated at around 2000 K. In case that the initial solid/liquid interfaces were (1 0 0) plane at the edge and the middle along [1 0 0] direction in $10 \times 5 \times 5$ supercell, the melting point was also determined to be around 2000 K.

Even in this method, a little overestimation of the melting point was observed since the experimental value of the melting point ranges between 1953 and 1993 K [18]. However, the overestimation is reasonable because thermally induced defects are not fully included in simulation and the volume of simulation cell having the solid/liquid interfaces was fixed at the equilibrium value of the solid state. Therefore, we considered that the simulation result was appropriate. As discussed in Section 3.4, proper simulation results in high temperatures can result from the fact that structures in which atoms are largely displaced were taken into account in the model construction.

3.6. Limitations and room for improvement in the present method

The validity and effectiveness of the present method were demonstrated through creation of potential models for $LiAlO_2$. However, some limitations, which should be improved, appeared.

First, the potential model that had the smallest fitting error did not always give material properties of the smallest error. This is because the fitting quality of potential energies in response to small distortions, which is important for evaluation of elastic properties, lessens, when we added potential energies of strongly distorted systems into fitting targets in order to achieve a good behavior at high temperatures. Namely, the accuracy of high-temperature properties such as thermal expansion and melting point was prone to be a trade-off with that of static properties such as elastic properties. This kind of trade-off is caused by that the model function cannot adequately reproduce potential energy responses for small and strong distortions simultaneously. Therefore it may be solved by sophisticating the model function.

There are some possible improvement ways in this line. One is inclusion of three-body interactions into Eq. (1) because contribution of three-body interaction is expected in $LiAlO_2$, in analogy

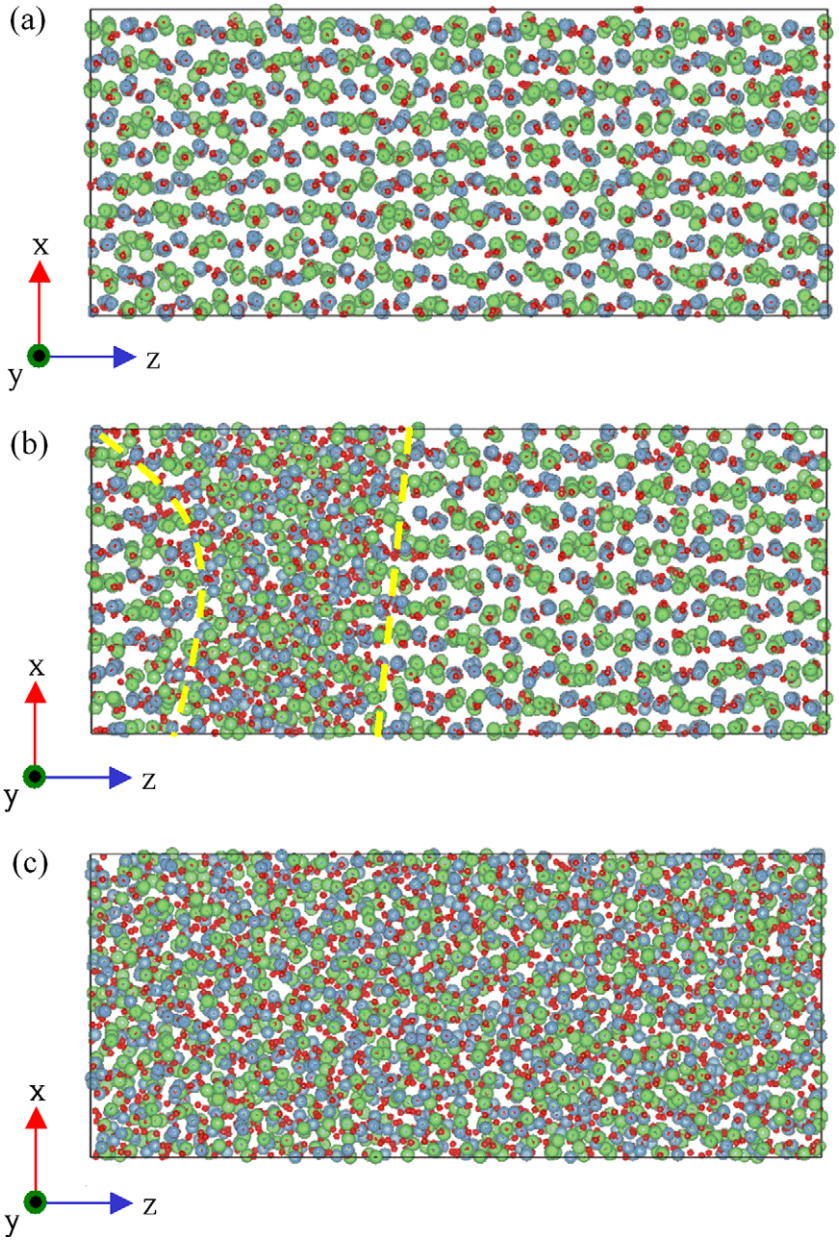

Fig. 7. Atomic configurations of the system after MD simulation for 1 ns at (a) 1900, (b) 2000 and (c) 2100 K. Green balls are Li, blue Al and red O. The yellow dashed lines in (b) indicate the solid–liquid interfaces. (For interpretation of the references to colour in this figure legend, the reader is referred to the web version of this article.)

with $LiNbO_3$ [22] as mentioned in Section 3.2. Another is combination with a variable-charge model [26]. As shown in Table 2, while "Optimized" values that are the results in the optimized $LiAlO_2$ structure were adopted as fixed in this research, they changed substantially under distorted conditions. Therefore, combination with a variable-charge model could be effective to improve our potential models.

Another shortcoming is that too large N (too many terms) in Eq. (1) causes improper extreme values in a potential as showed in Fig. 2. There are two possible reasons about this. One reason is again the absence of many-body interactions. A part of interaction that is expected to be described by many-body interactions could be expressed forcibly by pairwise potential as mentioned in Section 3.1. Therefore, inclusion of three-body interactions can relieve the problem. Combination with a variable-charge model may be effective as well. The other reason is the shortage of fitting targets in comparison with the number of parameters (degree of freedom) in Eq. (1). In this case, in addition to increase of fitting targets, selection method of effective fitting targets should be constructed.

Although these limitations remain, the present model successfully created a potential model for $LiAlO_2$. This result could be from the high ionicity of $LiAlO_2$. For application to other candidate breeders, especially for Li–Si–O systems where covalent interaction is expected to emerge strongly, addition of many-body interactions would be needed.

4. Conclusions

A method to construct interatomic potentials of which the optimized parameters are obtainable as a solution of simultaneous linear equations was presented. Potential models of $LiAlO_2$ were constructed. Consequently, the validity of our method was indicated through MS and MD simulation on material properties of $LiAlO_2$. This method can be applied to other Li-containing oxides,

although there are some limitations of the present model related to selection of fitting targets, ionic charges and effects of many-body interactions.

References

[1] M. Oyaidzu, Y. Morimoto, H. Kodama, M. Sasaki, H. Kimura, K. Munakata, M. Okada, K. Kawamoto, H. Moriyama, M. Nishikawa, K. Okuno, J. Nucl. Mater. 329–333 (2004) 1313.
[2] M. Oyaidzu, H. Kimura, A. Yoshikawa, Y. Nishikawa, K. Munakata, M. Okada, M. Nishikawa, K. Okuno, Fusion Eng. Des. 81 (2006) 583.
[3] V. Kapychev, V. Tebus, V. Frolov, J. Nucl. Mater. 307–311 (2002) 823.
[4] J.G. Rodeja, M. Meyer, M. Hayoun, Model. Simul. Mater. Sci. Eng. 9 (2001) 81.
[5] V. Milman, B. Winkler, J.A. White, C.J. Pickard, M.C. Payne, E.V. Akhmatskaya, R.H. Nobes, Int. J. Quant. Chem. 77 (2000) 895.
[6] J.P. Perdew, K. Burke, M. Ernzerhof, Phys. Rev. Lett. 77 (1996) 3865.
[7] A. de Vita, I. Manassidis, J.S. Lin, M.J. Gillan, Europhys. Lett. 19 (1992) 605.
[8] B.B. Karki, L. Stixrude, S.J. Clark, M.C. Warren, G.J. Ackland, J. Crain, Am. Mineral. 82 (1997) 635.
[9] P. Ewald, Ann. Phys. 64 (1921) 253.
[10] J.P. Biersack, J.F. Ziegler, Nucl. Instrum. Meth. 194 (1982) 93.
[11] R.S. Mulliken, J. Chem. Phys. 23 (1955) 1833.
[12] R.F.W. Bader, T.T. Nguyen-Dang, Y. Tal, Rep. Prog. Phys. 44 (1981) 893.
[13] J.D. Gale, J. Chem. Soc. Faraday Trans. 93 (1997) 629.
[14] T.R. Forester, W. Smith, DL_POLY User Manual, 1995.
[15] H.J.C. Berendsen, J.P.M. Postma, W.F. van Gunsteren, A. DiNola, J.R. Haak, J. Chem. Phys. 81 (1984) 3684.
[16] B.B. Laird, A.D.J. Haymet, Chem. Rev. 92 (1992) 1819.
[17] S. Izvekov, M. Parrinello, C.J. Burnham, J.G.A. Voth, Chem. Phys. 120 (2004) 10896.
[18] B. Cockayne, B. Lent, J. Cryst. Growth 54 (1981) 546.
[19] M.M.C. Chou, H.C. Huang, Appl. Phys. Lett. 88 (2006) 161906.
[20] F. Jachmann, M. Pattabiraman, C. Hucho, J. Appl. Phys. 98 (2005) 73501.
[21] J.F. Nye, Physical Properties of Crystals, Oxford University Press, Oxford, 1957.
[22] R.A. Jackson, M.E.G. Valerio, J. Phys.: Condens. Matter 17 (2005) 837.
[23] J. Zou, S. Zhou, J. Xu, L. Zhang, J. Appl. Phys. 98 (2005) 84909.
[24] S.M. Foiles, J.B. Adams, Phys. Rev. B 40 (1989) 5909.
[25] A.J.C. Ladd, L.V. Woodcock, Chem. Phys. Lett. 51 (1977) 155.
[26] V. Swamy, J.D. Gale, Phys. Rev. B 62 (2000) 5406.